Chapter 9
Defects in Indium-Related Nitride Compounds and Structural Design of AlN/GaN Superlattices

Kenji Shiraishi

In this chapter, we focus on two topics related to the electronic and optical properties of III-nitride compounds. By applying of ab initio approach, we can analyze the electronic structures of III-nitride compounds as well as other semiconductors. This is exemplified by theoretical analysis of electronic structures of In-related nitride compounds, which exhibit characteristic behavior originating from the large difference in the covalent radius between In and N atoms. By considering atomic and electronics structures of nitrogen vacancy (V_N) in InGaN in detail, the second nearest neighbor In–In interaction are crucial for unusually narrow bandgap of InN. Furthermore, this approach is applied to demonstrate AlN/GaN superlattice in the wurtzite phase with one or two GaN monolayers, which is efficient for near-band-edge c-plane emission of deep-ultraviolet (UV) LEDs. In particular, the emission wavelength is estimated to be 224 nm for the AlN/GaN superlattice with one GaN-monolayer, which is remarkably shorter than that for Al-rich AlGaN alloys. The optical matrix element of such superlattice is found to be 57% relative to the GaN bulk value. In Sect. 9.1, the atomic and electronic structures of V_N in InGaN to clarify the physical origin of the unusually narrow bandgap of InN. Section 9.2 is devoted to discuss structural design of AlN/GaN superlattices for deep-ultraviolet light-emitting diodes with high emission efficiency.

9.1 Defects in Indium-Related Nitride Compounds

In-related nitride compounds such as InGaN have attracted great attention from both technological and scientific viewpoints since InGaN is applied as a key material for blue light-emitting diodes [1]. Although it has been practically used in

K. Shiraishi (✉)
Institute of Materials and Systems for Sustainability, Nagoya University, Nagoya, Japan
e-mail: shiraishi@cse.nagoya-u.ac.jp

T. Matsuoka and Y. Kangawa (eds.), *Epitaxial Growth of III-Nitride Compounds*,
Springer Series in Materials Science 269,
https://doi.org/10.1007/978-3-319-76641-6_9

the semiconductor industry, many fundamental phenomena observed in In-related nitride compounds are still mysterious. The physical origin of the unusually narrow bandgap of InN [2–4] has not been clearly explained: the very small bandgap has been obtained in previous ab initio calculations [5]. In order to clarify the origin of the peculiar properties, it should be noted that the covalent radius of an In atom (1.44 Å) is much larger than that of an N atom (0.7 Å). This characteristic feature results in the relatively shorter distance between the second nearest neighbor In atoms as schematically shown in Fig. 9.1. As shown in this figure, the In–In distance in InN (3.5 Å) is much smaller than that in the typical covalent semiconductor of InAs (4.28 Å) due to the small covalent radius of N. It should also be noted that the In–In distance in a bulk In metal is 3.25 Å. These structural characteristics imply that the second nearest neighbor In–In interaction is of importance in In-related nitride compounds. It is thus expected that V_N in InGaN should reflect the importance of the In–In interaction.

The analysis of electronic structures of V_N for various atomic configuration in InGaN demonstrates that the second nearest neighbor In–In interaction is crucial as well as the nearest neighbor In–N interaction in In-related nitride compounds. Figure 9.2 shows the schematics of atomic configurations of V_N in InGaN considered in ab initio calculations. The calculated formation energy of V_N, which is defined as the minimum energy cost to generate V_N by removing N atom in InGaN, [6, 7] reveals that the formation energy of positively charged V_N is lower than that with neutral charge state. The calculated formation energy of V_N in n-type GaN is 2.84 eV under Ga-rich condition, where the chemical potential of N is assumed using (4.2), agrees with that in previous calculations [8]. Table 9.1 shows the relative formation energies of positively charged V_N. The formation energy in pure GaN is set to be zero for comparison. It is found that the formation energy decreases with the number of neighboring In atoms. The single substitution of In atom causes the decrease in the formation energy by $\sim$0.5 eV. Consequently, substitution of two In atoms for two Ga atoms results in the 1.0 eV decrease in the formation

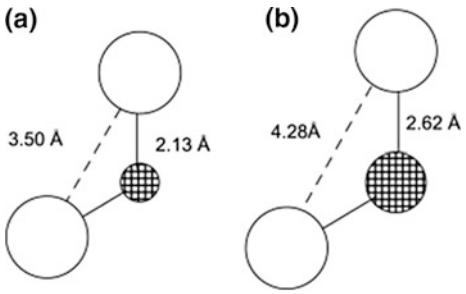

Fig. 9.1 Schematic illustration of the importance of the second nearest neighbor by considering the strong second nearest neighbor In–In interactions in In-related nitride semiconductors (**a**) compared with a conventional semiconductor of InAs (**b**). The open, small hatched and large hatched circles indicate In, N, and As atoms, respectively. Reproduced with permission from Obata et al. [12]. Copyright (2009) by Elsevier

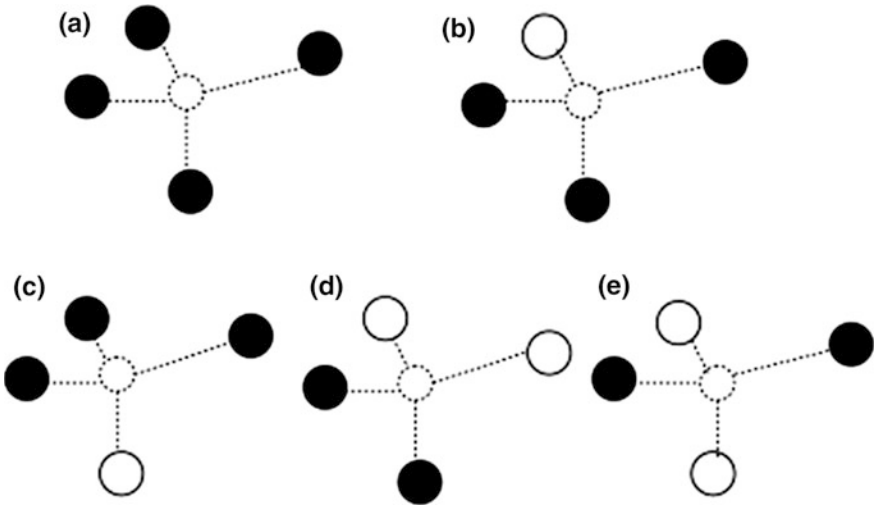

Fig. 9.2 Schematic illustration of the five investigated N mono-vacancy (V_N) structures. **a** V_N in perfect GaN, **b** V_N with one nearest neighbor In atom (Type I), **c** V_N with one nearest neighbor In atom (Type II), and **d** V_N with two nearest neighbor In atoms (Type I). The open and filled circles indicate In and Ga atoms, respectively and the open circle with the broken line corresponds to N mono-vacancies. Reproduced with permission from Obata et al. [12]. Copyright (2009) by Elsevier

Table 9.1 Relative formation energies of V_N in InGaN compared with the V_N formation energy in pure GaN. Atomic configuration of V_N in InGaN are shown in Fig. 9.2

Type of V_N	Formation energy (eV)
Pure GaN	0.0
One In (Type I)	−0.57
One In (Type II)	−0.50
Two In (Type I)	−1.05
Two In (Type II)	−0.96

energy of V_N. In covalent semiconductors, the formation energy of the vacancy is generally discussed in terms of a dangling bond counting model [9, 10]. The formation energy corresponds to the energy cost to disrupt the four bonds around the vacancy. Therefore, it is considered that the decrease in the formation energy corresponds to the energy difference between Ga–N and In–N. However, the energy gains by the formation of Ga–N and In–N bonds are estimated as 2.26 and 1.99 eV, respectively [11]. The estimated value of the decrease of the formation energy is (0.27 eV) is only half of the calculated value ($\sim$0.5 eV). This indicates that additional energy gain of 0.23 eV are important in InGaN.

To clarify the origin of the above discrepancy, the atomic structures of V_N with two nearest neighbor In atoms have been investigated. Figure 9.3a shows the schematics of atomic positions of In and N atoms around V_N along with the calculated contour plots of total charge density of InGaN with V_N [12]. As shown in

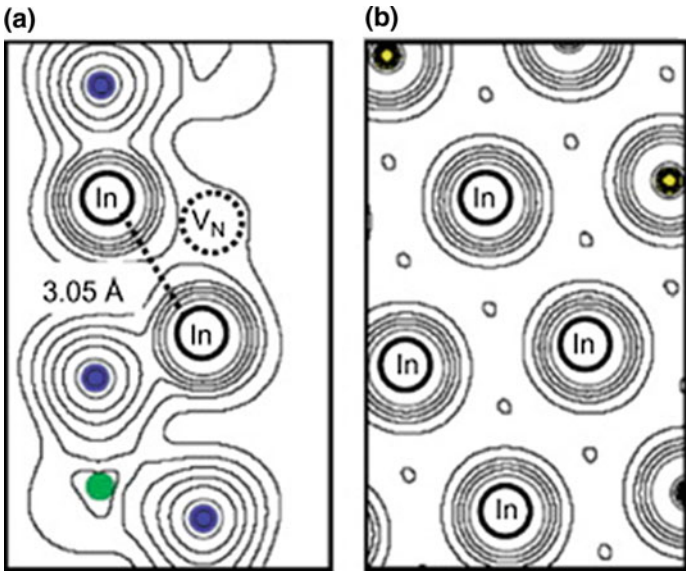

Fig. 9.3 Contour plots of total charge density. **a** InGaN with V_N, and **b** bulk In metal. The open circle with solid line corresponds to In atoms and the open circle with broken line indicates N mono-vacancies. Each contour represents twice (or half) of the density of the adjacent contour lines. The lowest values represented by the contour is 0.11 Å. Reproduced with permission from Obata et al. [12]. Copyright (2009) by Elsevier

Fig. 9.3a, the calculated In–In distance, which is originally the second nearest neighbor atoms, is only 3.05 Å. This value is even smaller than the In–In distance in bulk In (3.25 Å), indicating a strong interaction between the second nearest neighbor In–In atoms. In fact, the total charge density shown in Fig. 9.3a reflects the strong interaction between In atoms. From the calculated contour plots bulk In shown Fig. 9.3b, it is also found that the In–In interaction in InGaN with V_N is much stronger than that in bulk In, i.e., the In–In bond generated around V_N is much stronger than the In–In bond in bulk In, indicating that the concept of dangling bonds which is relevant in the conventional semiconductors is insufficient in InGaN. The formation of strong In–In bond is qualitatively consistent with theoretical reports that multiple N vacancies in InN cause metallic bonding between In–In atoms in InN [13]. Furthermore, the formation metallic In–In bonds is estimated to be 0.4 eV. This value is sufficient to explain above mentioned the additional energy gain of 0.23 eV. Moreover, the energy gain reduction of 0.17 eV seems to be natural by considering the fact that In–In bond formation in InGaN induces energetically unfavorable lattice distortion around V_N. Therefore, it is necessary to adopt a new material concept that the second nearest neighbor interaction between In atoms is very important as well as the nearest neighbor interaction for considering In-related nitride compounds.

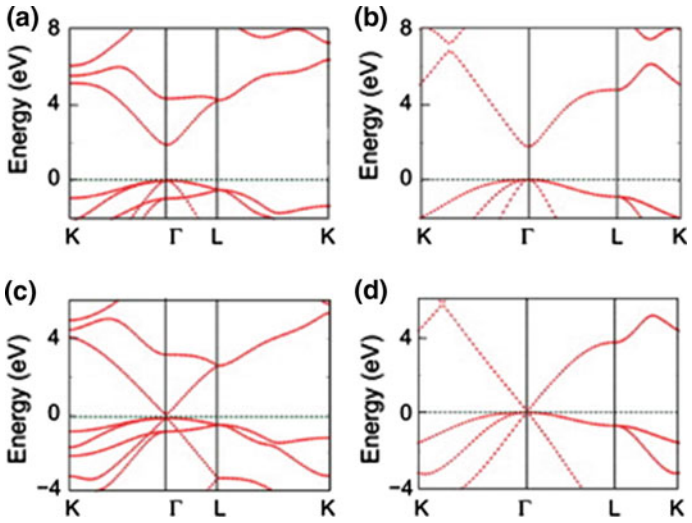

Fig. 9.4 Band structures of **a** wurtzite GaN, **b** zinc-blende GaN, **c** wurtzite InN, and **d** zinc-blende InN. The energy of valence band top is set to zero. Reproduced with permission from Obata et al. [12]. Copyright (2009) by Elsevier

By considering the second nearest neighbor In–In interactions, the physical origin of the unusually narrow bandgap of InN can be explained. In the wurtzite structure, each In atom is surrounded by 4 nearest neighbor N atoms and 12 nearest neighbor In atoms. Figure 9.4 shows the band structures of GaN and InN with both wurtzite and zinc-blende structures. As shown in these figures, InN bandgaps are much smaller than GaN for both the wurtzite and zinc-blende structures. It is noticeable that InN bandgaps become smaller due to the large dispersions of the conduction bands (especially around Γ point) for both wurtzite and zinc blende structures. This large dispersion corresponds to the very small electron effective mass of InN. Since both the wurtzite and zinc blende band structures have similar characteristics, and since the atomic configurations of the wurtzite and zinc blende structures are the same within the second nearest neighbor atoms, it is sufficient to just consider the zinc blende band structure in order to clarify the physical origin of the narrow bandgap in InN. In zinc-blende structures, the energy level at the Γ point can be described analytically based on the tight-binding calculations [14]. If we consider only the nearest neighbor interactions, the energy of the conduction band bottom at the Γ point, $E(\Gamma^c)$, is expressed as

$$E(\Gamma^c) = \frac{E(\mathrm{In}, s) + E(\mathrm{N}, s)}{2} + \sqrt{\left(\frac{E(\mathrm{In}, s) - E(\mathrm{N}, s)}{2}\right)^2 + 16t^2(\mathrm{In}, s : \mathrm{N}, s)}, \quad (9.1)$$

where, $E(\mathrm{In}, s)$ and $E(\mathrm{N}, s)$ are the on-site energies of the In-5s and N-2s orbitals, respectively, and $t(\mathrm{In}, s : \mathrm{N}, s)$ is the transfer integral between In-5s and

N-2s orbitals. In addition to the nearest neighbor interactions, we can easily include the interaction between second nearest neighbor In atoms. The obtained energy of the conduction band bottom at the Γ point, $E'(\Gamma^c)$ can be written as

$$E'(\Gamma^c) = \frac{E(\mathrm{In},s) + 12t(\mathrm{In},s:\mathrm{In},s) + E(\mathrm{N},s)}{2} + \sqrt{\left(\frac{E(\mathrm{In},s) + 12t(\mathrm{In},s:\mathrm{In},s) - E(\mathrm{N},s)}{2}\right)^2 + 16t^2(\mathrm{In},s:\mathrm{N},s)}, \tag{9.2}$$

where $t(\mathrm{In},s:\mathrm{In},s)$ is the transfer integral between the second nearest neighbor In-5s orbitals. As shown in (9.1) and (9.2), it is naturally concluded that the energy of the conduction band bottom should drastically decrease when the magnitude of negative value of $t(\mathrm{In},s:\mathrm{In},s)$ is sufficiently large, leading to an extremely narrow bandgap. To roughly estimate the transfer integral between second nearest neighbor In atoms, $t(\mathrm{In},s:\mathrm{In},s)$, for InN and InAs, we calculated the hypothetical In_2 molecules whose distances correspond to InN (3.50 Å) and InAs (4.28 Å), respectively. The calculated values of bonding–antibonding splittings of In-5s orbitals are 1.2 and 0.4 eV for 3.50 and 4.28 Å, respectively. Therefore, it is expected that $t(\mathrm{In},s:\mathrm{In},s)$ of InN is three times larger than that of InAs. This implies that second nearest In–In interaction is much more significant in InN than that in InAs. Moreover, it is also concluded that the decrease in the conduction band energy which originates from the second nearest neighbor In–In interaction is three times larger in InN than that in InAs. Since the strong In–In interaction governs the band width, it is concluded that the band dispersion of the conduction band should be large. The unusually narrow bandgap of InN can naturally be explained by considering the strong second nearest neighbor In–In interactions.

9.2 Structural Design of AlN/GaN Superlattices for Deep-UV LEDs with High Emission Efficiency

The UV LEDs have recently attracted a great deal of attention as promising candidates for the next-generation high-density optical storage and solid-state lighting. Recently, fabrication of deep-UV AlN LEDs has been reported with an emission efficiency of 1×10^{-4} % [15–21]. However, this emission efficiency is still much lower than that of the near-UV GaN LED. This is because AlN has an anisotropic emission pattern where light is emitted barely from the (0001) planes (c-plane), but preferentially from the $(11\bar{2}0)$ planes (a-plane). An increase in its emission efficiency is thus necessary for practical application of deep-UV AlN LEDs.

The directional light emission properties of AlN LEDs reflect a different valence band structure for AlN compared with that of GaN, as described in Sect. 3.2

[22–24] In general, the valence bands at the Γ point for wurtzite crystals such as AlN and GaN are separated into heavy-hole (HH), light-hole (LH), and crystal-field-split-off hole (CH) bands due to spin-orbit interactions and the crystal field. The HH and LH states have a character of nitrogen 2p orbitals perpendicular to the c-axis, while the CH state is characterized by nitrogen 2p orbitals parallel to the c-axis. The optical transitions between the HH or LH bands and the conduction band are mainly allowed for light polarized perpendicular to the c-axis ($\mathbf{E}\perp$c), where $\mathbf{E}$ is the electric field vector of the emitted light. On the other hand, the transition between the CH band and the conduction band is predominantly allowed for light polarized parallel to the c-axis ($\mathbf{E} \parallel$ c).

In GaN, the HH and LH bands are higher in energy than the CH with crystal-field splitting Δ_{cf} of $\sim$25 meV [25, 26]. By contrast, in AlN, the CH band is energetically higher than the HH and LH bands, which leads to negative crystal-field splitting Δ_{cf} of -165 meV [21]. The difference in electronic structure between AlN and GaN results in the anisotropic emission pattern of the AlN. Therefore, to increase the efficiency of the c-plane surface emission in deep-UV AlN LEDs, the important issue is how to convert the negative Δ_{cf} to positive. For this purpose, the conventional method is using the ternary alloy of AlGaN. It has been reported, however, that the Ga composition at which Δ_{cf} becomes zero is 22–27%, [27] which limits its c-plane emission wavelength to $\sim$240–260 nm. To obtain near-band-edge c-plane emission of deep-UV LEDs, we consider a [0001]-oriented AlN/GaN superlattice in the wurtzite phase. The period of the superlattice along the [0001] direction (c-axis) was fixed to be 20 monolayers, i.e., $(AlN)_{20-n}/(GaN)_n$, where n is the number of monolayers ($n = 1, \ldots, 10$), is taken into account as a representative of [0001]-oriented AlN/GaN superlattice. Figure 9.5 shows the structural model of the AlN/GaN superlattices.

Figure 9.6 shows the electronic energy bands of the $(AlN)_{20-n}/(GaN)_n$ superlattices around the Γ point. In the AlN bulk, corresponding to $n = 0$, the CH band is energetically higher than the HH and LH bands, which leads to a negative of -0.23 eV [28]. It should be noted that the HH and LH bands are degenerate at the Γ point because the spin-orbit coupling is neglected. In the AlN/GaN superlattices, the HH and LH bands are, however, higher in energy than the CH band, resulting in the valence band top. The calculated Δ_{cf} as a function of the number of GaN monolayers shown in Fig. 9.7 [28] exhibits the reverse of the Δ_{cf} sign for AlN/GaN superlattices with more than one GaN monolayer. The calculated Δ_{cf} is about +0.18 eV in the $(AlN)_{19}/(GaN)_1$ superlattice. Furthermore, the value of Δ_{cf} increases with GaN thickness, but it approaches +0.40 eV in the AlN/GaN

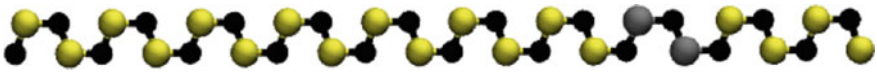

Fig. 9.5 Structural model of AlN/GaN superlattices.The figure shows $(AlN)_{18}/(GaN)_2$ as an example. Yellow, black, and gray circles represent Al, N, and Ga atoms, respectively. Reproduced with permission from Kamiya et al. [28]. Copyright (2012) by the Japan Society of Applied Physics

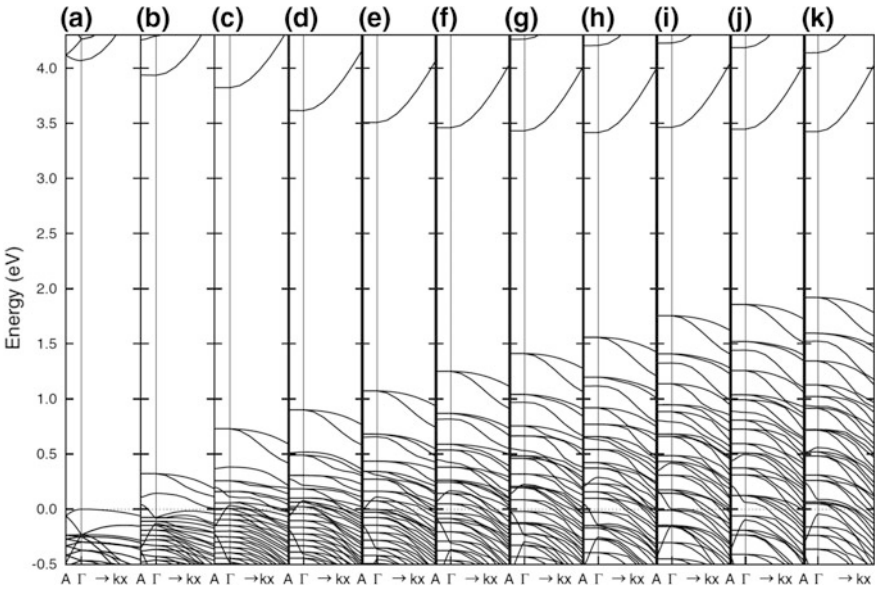

Fig. 9.6 Energy band structure around the Γ point of the **a** bulk AlN,c Energies are measured from the valence band top of bulk AlN at the Γ point. Reproduced with permission from Kamiya et al. [28]. Copyright (2012) by the Japan Society of Applied Physics

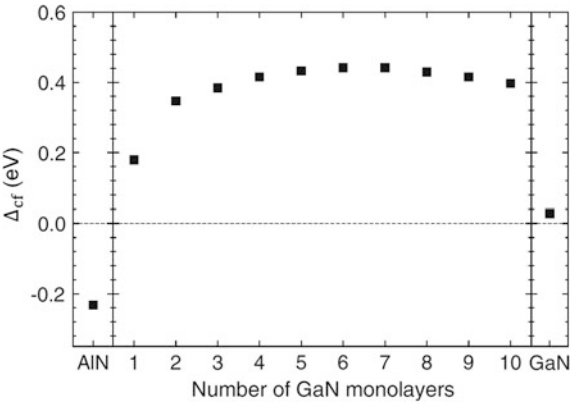

Fig. 9.7 Calculated crystal-field splitting Δ_{cf} of a AlN/GaN superlattice as a function of the number of GaN monolayers. Reproduced with permission from Kamiya et al. [28]. Copyright (2012) by the Japan Society of Applied Physics

superlattices with more than three GaN monolayers. These results indicate clearly that a negative value of Δ_{cf} in the AlN bulk is converted to a positive value of Δ_{cf} by using the AlN/GaN superlattice with more than one GaN monolayer.

Figure 9.8 shows the wave functions of the lowest conduction band, HH/LH bands, and CH band for the $(AlN)_{20-n}/(GaN)_n$ superlattices [28]. It is found that the wave functions in the HH and LH bands are characterized by N 2p orbitals

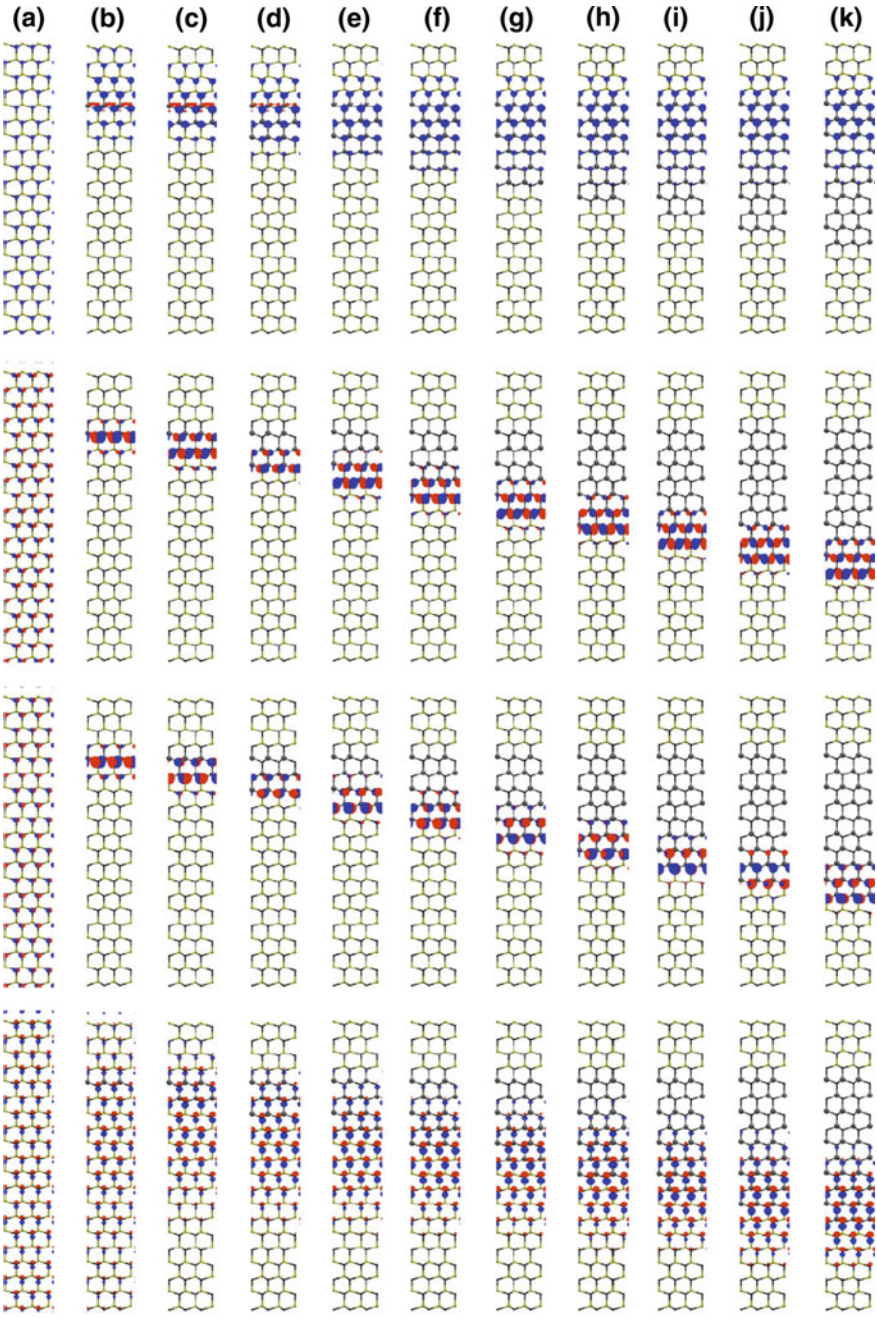
(a)
(b)
(c)
(d)
(e)
(f)
(g)
(h)
(i)
(j)
(k)

◂**Fig. 9.8** Isosurfaces of the wavefunctions in the (upper) lowest conduction band, (two middle) HH/LH bands, and (lower) CH band at the Γ point for the **a** bulk AlN, **b** $(AlN)_{19}/(GaN)_1$, **c** $(AlN)_{18}/(GaN)_2$, **d** $(AlN)_{17}/(GaN)_3$, **e** $(AlN)_{16}/(GaN)_4$, **f** $(AlN)_{15}/(GaN)_5$, **g** $(AlN)_{14}/(GaN)_6$, **h** $(AlN)_{13}/(GaN)_7$, **i** $(AlN)_{12}/(GaN)_8$, **j** $(AlN)_{11}/(GaN)_9$, and **k** $(AlN)_{10}/(GaN)_{10}$ superlattices. Blue and red isosurfaces represent positive and negative values, respectively. The isovalues are ± 1.08 $(e/Å^3)^{1/2}$. Reproduced with permission from Kamiya et al. [28]. Copyright (2012) by the Japan Society of Applied Physics

perpendicular to the c-axis, while the wave function in the CH band has a character of N-2p orbitals parallel to the c-axis; the lowest conduction state is composed mainly of N-2*s* orbitals. We also found that the wave functions in the HH, LH, and lowermost conduction bands are much more localized in a quantum well than that in the CH band. This demonstrates that quantum confinement effects are larger for the former three bands than the latter. This difference in the confinement effects is also observed in the band structures shown in Fig. 9.6, where the HH and LH bands in the AlN/GaN superlattice have a flat dispersion along the Γ to A line (k_z direction), while the CH band has a small dispersion along this direction. On the other hand, all of these bands have a significant dispersion along the k_x direction in all the AlN/GaN superlattices. The calculated electron and hole effective masses are listed in Table 9.2. These results clearly provide evidence that the negative Δ_{cf} is reversed in the AlN/GaN superlattice due to the difference in quantum confinement effects between the HH/LH and CH bands.

From Fig. 9.6, it is also found that the high-lying valence bands and the low-lying conduction bands in the AlN/GaN superlattice shift upward and downward, respectively, with GaN thickness. The energy gap of the AlN/GaN superlattices with one to five GaN monolayers is ranging within the deep-UV spectral region. In particular, the bandgap is found to be 5.5 eV (224 nm) and 5.0 eV (247 nm) in $(AlN)_{19}/(GaN)_1$ and $(AlN)_{18}/(GaN)_2$, respectively. The confinement effects lead to the monotonic decrease in the energy gap. Moreover, as can be seen in Fig. 9.8, the wave functions in the valence bands and the conduction band are separately distributed in a quantum well. These phenomena are ascribed to the quantum-confinement Stark effect (QCSE), in which the built-in electric field across the quantum well exists in the AlN/GaN superlattice. This electric field tends to separate an electron and a hole localized in a quantum well, as clearly indicated by

Table 9.2 Electron and hole effective masses (m_e and m_h, respectively) for an AlN/GaN superlattice as a function of the number of GaN monolayers. The $\perp$ and $\parallel$ denote the components along the k_x and k_x directions, respectively. All values are measured in units of a free-electron mass m_0

	AlN	1	2	3	4	5	6	7	8	9	10	GaN
$m_e^{\perp}$	0.31	0.33	0.33	0.32	0.30	0.30	0.29	0.29	0.29	0.29	0.29	0.18
$m_e^{\parallel}$	0.30											0.17
$m_h^{\perp}$	4.02	1.70	1.71	1.73	1.74	1.74	1.76	1.76	1.78	1.78	1.79	2.29
$m_h^{\parallel}$	0.25											2.23

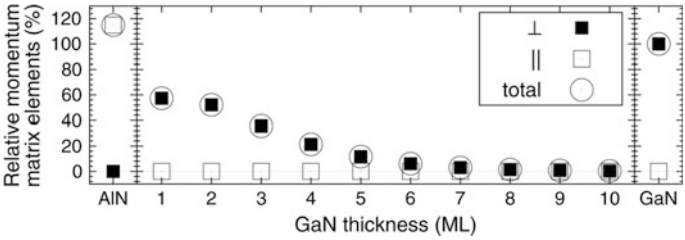

Fig. 9.9 Interband optical momentum matrix elements of an AlN/GaN superlattice as a function of GaN monolayer thickness, calculated at the C point between the highest valence band and the lowest conduction band. All the values are normalized to the square value of the momentum matrix element for GaN bulk. The ⊥ and ∥ denote the components that are perpendicular and parallel to the c-axis, respectively. Reproduced with permission from Kamiya et al. [29]. Copyright (2011) by American Institute of Physics

the distribution of the square of the wave functions in the valence band top and conduction band bottom in Fig. 9.8. It is thus suggested that the AlN/GaN superlattice with one or two GaN monolayers is efficient for near-band-edge emission of a deep-UV LED. It should be noted that using different AlN thicknesses for the AlN/GaN superlattice, i.e., $(AlN)_{29}/(GaN)_1$ and $(AlN)_{39}/(GaN)_1$, gives the same results as with $(AlN)_{19}/(GaN)_1$: The results are independent of AlN thickness.

Figure 9.9 shows the interband optical momentum matrix element of the AlN/GaN superlattice as a function of Ga monolayer thickness, also shown in AlN bulk and GaN bulk cases; these values are shown as a relative value to that of GaN, $r_{\text{superlatice/GaN}}$, given by

$$r_{\text{superlattice/GaN}} = \frac{|\psi_c|\mathbf{P}|\psi_v|_{\text{AlN/GaN}}}{|\psi_c|\mathbf{P}|\psi_v|_{\text{GaN}}}, \tag{9.3}$$

where ψ_v and ψ_c are the wave functions of the valence band top and conduction band bottom at the Γ point, respectively, $\mathbf{P}$ is the momentum operator, and subscripts AlN/GaN and GaN in momentum matrix elements denote AlN/GaN superlattice and bulk GaN, respectively [29]. In the case of the AlN bulk, the component of the matrix element perpendicular to the c-axis is almost equal to zero, and the matrix element component parallel to the c-axis accounts for a majority of the total. The trend is completely opposite in the case of the GaN bulk. However, the component of the matrix element perpendicular to the c-axis significantly increases for the AlN/GaN superlattices with one and two GaN monolayers, as shown in Fig. 9.9. The calculated values are 57 and 52% relative to GaN bulk for the $(AlN)_{19}/(GaN)_1$ and $(AlN)_{18}/(GaN)_2$ cases, respectively. On the other hand, the component parallel to the c-axis is almost down to zero in all of the AlN/GaN superlattices. The momentum matrix elements decrease monotonically as the number of GaN monolayers increases. This monotonic decrease originates from the

QCSE. These results offer the improvement of near-band-edge emission from the c-plane by using AlN/GaN superlattices.

On the basis of these calculated results, it is concluded that quantum confinement effects of the AlN/GaN superlattices with one and two GaN monolayers lead to spreading the energy gap of GaN bulk as well as reversing the negative Δ_{cf} in AlN bulk: such a superlattice structure makes the best use of both the high emission efficiency of GaN up to 57% in terms of the optical matrix element and the wide energy gap of AlN up to 5.5 eV (224 nm). Since 22–27% Ga composition in ternary alloy of AlGaN is needed to reverse the Δ_{cf} sign, [27] which limits the emission wavelength to ~ 240–260 nm, this is the advantageous of using superlattices compared with using the ternary alloy of AlGaN.

References

1. S. Nakamura, M. Senoh, S. Nagahama, N. Iwasa, T. Yamada, T. Matsushita, H. Kiyoku, Y. Sugimoto, InGaN-based multi-quantum-well-structure laser diodes. Jpn. J. Appl. Phys. **37**, L74 (1996)
2. T. Matsuoka, H. Okamoto, M. Nakao, H. Harima, E. Kurimoto, Optical bandgap energy of wurtzite InN. Appl. Phys. Lett. **81**, 1246 (2002)
3. V.Y. Davydov, A.A. Klochikhin, V.V. Emtsev, S.V. Ivanov, V.V. Vekshin, F. Bechstedt, J. Fürthmuller, H. Harima, A.V. Mudryi, A. Hashimoto, A. Yamamoto, J. Aderhold, J. Graul, E.E. Haller, Band gap of InN and In-rich $In_xGa_{1-x}N$ alloys ($0.36<x<1$). Phys. Status Solidi B **230**, R4 (2002)
4. Y. Nanishi, Y. Saito, T. Yamaguchi, RF-molecular beam epitaxy growth and properties of InN and related alloys. Jpn. J. Appl. Phys. **42**, 2549 (2003)
5. M. Usuda, N. Hamada, K. Shiraishi, A. Oshiyama, Band structures of wurtzite InN and $Ga_{1-x}In_xN$ by all-electron GW calculation. Jpn. J. Appl. Phys. **43**, L407 (2004)
6. M. Otani, K. Shiraishi, A. Oshiyama, First-principles calculations of boron-related defects in SiO_2. Phys. Rev. B. **68**, 184112 (2003)
7. D.J. Chadi, K.J. Chang, Magic numbers for vacancy aggregation in crystalline Si. Phys. Rev. B **38**, 1523 (1988)
8. C.G. Van de Walle, J. Neugebauer, First-principles calculations for defects and impurities: Applications to III-nitrides. J. Appl. Phys. **95**, 3851 (2004)
9. T. Akiyama, A. Oshiyama, O. Sugino, Magic numbers of multivacancy in crystalline Si: tight-binding studies for the stability of the multivacancy. J. Phys. Soc. Jpn. **67**, 4110 (1998)
10. T. Akiyama, A. Oshiyama, First-principles study of hydrogen incorporation in multivacancy in silicon. J. Phys. Soc. Jpn. **70**, 1627 (2001)
11. M. Fuchs, J.L.F. DaSilva, C. Stampfl, J. Neugebauer, M. Scheffler, Cohesive properties of group-III nitrides: A comparative study of all-electron and pseudopotential calculations using the generalized gradient approximation. Phys. Rev. B **65**, 245212 (2002)
12. T. Obata, J.-I. Iwata, K. Shiraishi, A. Oshiyama, First principles studies on In-related nitride compounds. J. Cryst. Growth **311**, 2772 (2009)
13. X.M. Duan, C. Stampfl, Nitrogen vacancies in InN: vacancy clustering and metallic bonding from first principles. Phys. Rev. B **77**, 115207 (2008)
14. K.E. Newman, J.D. Dow, Theory of deep impurities in silicon-germanium alloys. Phys. Rev. B **30**, 1929 (1984)
15. T. Nishida, N. Kobayashi, 346 nm emission from AlGaN multi-quantum-well light emitting diode. Phys. Status Solidi A **176**, 45 (1999)

16. V. Adivarahan, W.H. Sun, A. Chitnis, M. Shatalov, S. Wu, H.P. Maruska, M.A. Khan, 250 nm AlGaN light-emitting diodes. Appl. Phys. Lett. **85**, 2175 (2004)
17. M.A. Khan, M. Shatalov, H.P. Maruska, H.M. Wang, E. Kuokstis, III–nitride UV devices. Jpn. J. Appl. Phys. **44**, 7191 (2005)
18. Y. Taniyasu, M. Kasu, T. Makimoto, An aluminium nitride light-emitting diode with a wavelength of 210 nanometres. Nature (London) **441**, 325 (2006)
19. A.A. Yamaguchi, Anisotropic optical matrix elements in strained GaN quantum wells on semipolar and nonpolar substrates. Jpn. J. Appl. Phys. **46**, L789 (2007)
20. A.A. Yamaguchi, Valence band engineering for remarkable enhancement of surface emission in AlGaN deep-ultraviolet light emitting diodes. Phys. Status Solidi C **5**, 2364 (2008)
21. Y. Taniyasu, M. Kasu, Origin of exciton emissions from an AlN p-n junction light-emitting diode. Appl. Phys. Lett. **98**, 131910 (2011)
22. M. Suzuki, T. Uenoyama, A. Yanase, First-principles calculations of effective-mass parameters of AlN and GaN. Phys. Rev. B **52**, 8132 (1995)
23. S.-H. Wei, A. Zunger, Valence band splittings and band offsets of AlN, GaN, and InN. Appl. Phys. Lett. **69**, 2719 (1996)
24. K. Kim, W.R.L. Lambrecht, B. Segall, M. van Schilfgaarde, Effective masses and valence-band splittings in GaN and AlN. Phys. Rev. B **56**, 7363 (1997)
25. D.C. Reynolds, D.C. Look, W. Kim, Ö. Aktas, A. Botchkarev, A. Salvador, H. Morkoç, D.N. Talwar, Ground and excited state exciton spectra from GaN grown by molecular-beam epitaxy. J. Appl. Phys. **80**, 594 (1996)
26. I. Vurgaftman, J.R. Meyer, Band parameters for nitrogen-containing semiconductors. J. Appl. Phys. **94**, 3675 (2003)
27. H. Kawanishi, E. Niikura, M. Yamamoto, S. Takeda, Experimental energy difference between heavy- or light-hole valence band and crystal-field split-off-hole valence band in $Al_xGa_{1-x}N$. Appl. Phys. Lett. **89**, 251107 (2006)
28. K. Kamiya, Y. Ebihara, M. Kasu, K. Shiraishi, Efficient structure for deep-ultraviolet light-emitting diodes with high emission efficiency: a first-principles study of AlN/GaN superlattice. Jpn. J. Appl. Phys. **51**, 02BJ11 (2012)
29. K. Kamiya, Y. Ebihara, K. Shiraishi, M. Kasu, Structural design of AlN/GaN superlattices for deep-ultraviolet light-emitting diodes with high emission efficiency. Appl. Phys. Lett. **99**, 151108 (2011)